Proposed crystal structure of carbadox, $C_{11}H_{10}N_4O_4$

James A. Kaduk,[1,2,a] Anja Dosen,[3] and Thomas N. Blanton[3]
[1]*Illinois Institute of Technology, 3101 S. Dearborn St., Chicago, IL 60616, USA*
[2]*North Central College, 131 S. Loomis St., Naperville, IL 60540, USA*
[3]*ICDD, 12 Campus Blvd., Newtown Square, PA 19073-3273, USA*

(Received 26 October 2023; accepted 31 January 2024)

A model for the crystal structure of carbadox has been generated and refined using synchrotron X-ray powder diffraction data and optimized using density functional theory techniques. Carbadox crystallizes in space group $P2_1$ (#4) with $a = 13.8155(3)$, $b = 21.4662(1)$, $c = 16.3297(3)$ Å, $\beta = 110.0931(7)°$, $V = 4548.10(3)$ Å^3, and $Z = 16$. The crystal structure is characterized by approximately parallel stacking of the eight independent carbadox molecules parallel to the *bc*-plane. There are two different molecular configurations of the eight carbadox molecules; five are in the lower-energy configuration and three are in a ~10% higher-energy configuration. This arrangement likely achieves the lowest-energy crystalline packing via hydrogen bonding. Hydrogen bonds link the molecules both within and between the planes. Each of the amino groups forms a N–H···O hydrogen bond to an oxygen atom of the 1,4-dioxidoquinoxaline ring system of another molecule. The result is four pairs of hydrogen-bonded molecules, which form rings with graph set *R2,2(14)*. Variation in specimen preparation can affect the preferred orientation of particles considerably. The powder pattern has been submitted to ICDD for inclusion in the Powder Diffraction File™ (PDF®).

[doi:10.1017/S0885715624000083]

Keywords: carbadox, Mecadox®, crystal structure, Rietveld refinement, density functional theory

I. INTRODUCTION

Carbadox, $C_{11}H_{10}N_4O_4$ (sold under the brand name Mecadox, among others), is a veterinary antibiotic drug used to treat infections in swine, particularly dysentery. It has been shown to be carcinogenic and to cause birth defects in laboratory animals, resulting in its being banned in several countries.

The systematic name (CAS Registry Number 6804-07-5) is methyl *N*-[(E)-(1,4-dioxidoquinoxaline-1,4-diium-2-yl) methylideneamino]carbamate. A two-dimensional molecular diagram is shown in Figure 1. We are unaware of any published X-ray powder diffraction data on carbadox.

This work was carried out as part of a project (Kaduk et al., 2014) to determine the crystal structures of large-volume commercial pharmaceuticals and include high-quality powder diffraction data for them in the Powder Diffraction File (Gates-Rector and Blanton, 2019).

II. EXPERIMENTAL

Carbadox, a commercial reagent, was purchased from TargetMol (Batch #113752) and was used as-received. The yellow powder was packed into a 1.5 mm diameter Kapton capillary and rotated during the measurement at ~50 Hz. The powder pattern was measured at 295 K at beam line 11-BM (Antao et al., 2008; Lee et al., 2008; Wang et al., 2008) of the Advanced Photon Source at Argonne National Laboratory using a wavelength of 0.458208(2) Å from 0.5–50° 2θ with a step size of 0.001° and a counting time of 0.1 s/step. The high-resolution powder diffraction data were collected using twelve silicon crystal analyzers that allow for high angular resolution, high precision, and accurate peak positions. A mixture of silicon (NIST SRM 640c) and alumina (NIST SRM 676a) standards (ratio Al_2O_3:Si = 2:1 by weight) was used to calibrate the instrument and refine the monochromatic wavelength used in the experiment.

The pattern was initially indexed using DICVOL06 (Louër and Boultif, 2007) as incorporated into FOX (Favre-Nicolin

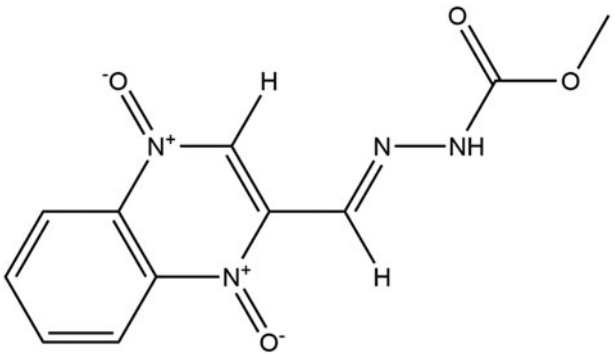

Figure 1. The 2D molecular structure of carbadox.

[a]Author to whom correspondence should be addressed. Electronic mail: kaduk@polycrystallography.com

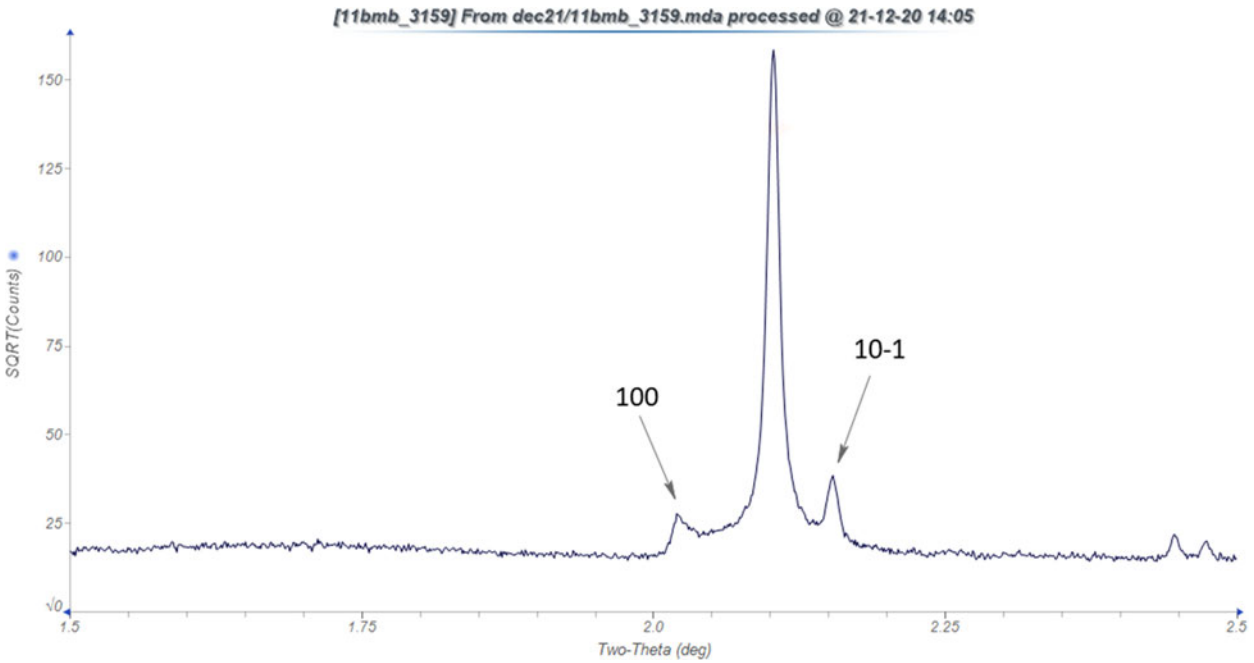

Figure 2. The low-angle portion of the carbadox diffraction pattern, illustrating the 100 and 10-1 peaks that violate glide planes and demonstrate that the space group is $P2_1$. Image generated using JADE Pro (MDI, 2023).

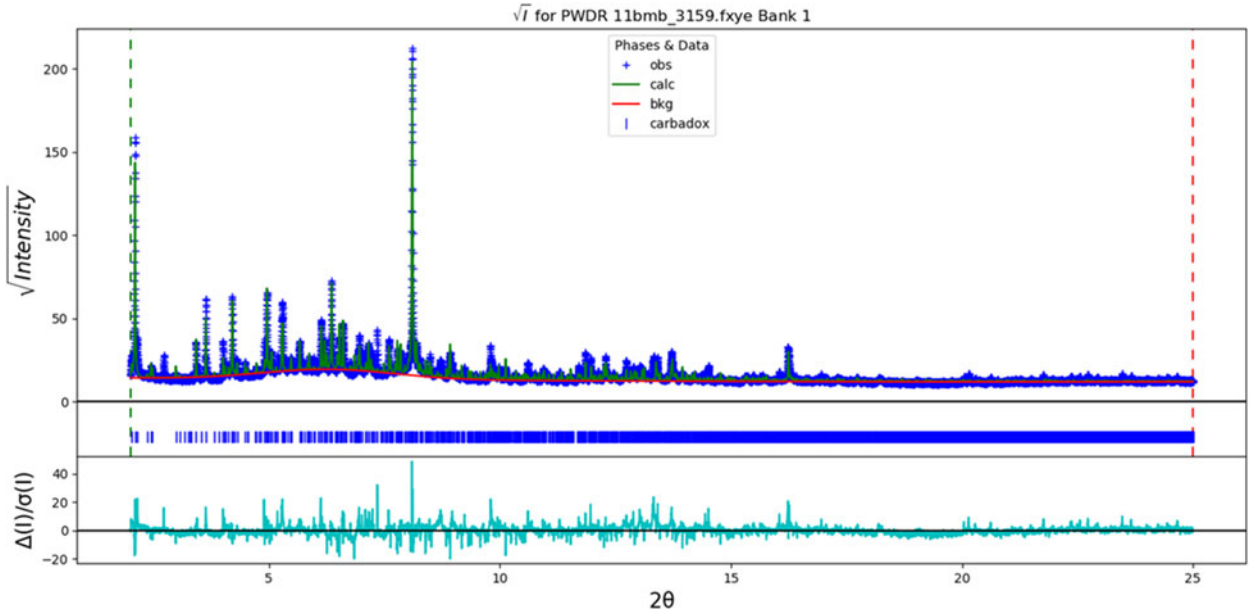

Figure 3. The Rietveld plot for the refinement of carbadox. The blue crosses represent the observed data points, and the green line is the calculated pattern. The cyan curve is the normalized error plot, and the red line is the background curve. The vertical scale is the square root of the intensities.

and Černý, 2002) on a primitive monoclinic unit cell with $a = 15.39751(22)$, $b = 21.47282(9)$, $c = 6.90792(10)$ Å, $\beta = 94.8164(10)°$, $V = 2275.888(18)$ Å^3, and $Z = 8$. The suggested space group was $P2_1/n$. A reduced cell search in the Cambridge Structural Database (Groom et al., 2016) yielded four hits but no carbadox derivatives.

The carbadox molecule was downloaded from PubChem (Kim et al., 2023) as Conformer3D_CID_135511839.sdf, converted to a *.mol2 file using Mercury (Macrae et al., 2020), and converted to a Fenske-Hall Z-matrix using OpenBabel (O'Boyle et al., 2011). Although a structure was obtained using FOX, the unit cell did not account for several peaks between 5° and 8° 2θ. The pattern was thus re-indexed using a larger number of peaks (31) with DICVOL14 (Louër and Boultif, 2014) on a primitive monoclinic unit cell with $a = 13.8212$, $b = 21.4595$, $c = 16.3396$ Å, $\beta = 110.097°$, $V = 4551.21$ Å^3, and $Z = 16$. This cell is among the 2× supercells

TABLE I. Powder structures in the CSD with different numbers of molecules in the asymmetric unit (Z').

Z'	1	2	3	4	5	6	7	8	9	10
#	3061	278	23	22	3	1	0	2	0	1

https://doi.org/10.1017/S0885715624000083 Published online by Cambridge University Press

TABLE II. Root-mean-square Cartesian displacements between the Rietveld-refined and DFT-optimized structures of carbadox molecules.

Molecule	11–57 odd	22–58 even	359–115 odd	460–116 even	5233–289odd	6234–290 even	7291–347 odd	8292–348 even
rms Δ, Å	0.204	0.411	0.601	0.562	0.232	0.187	0.321	0.328

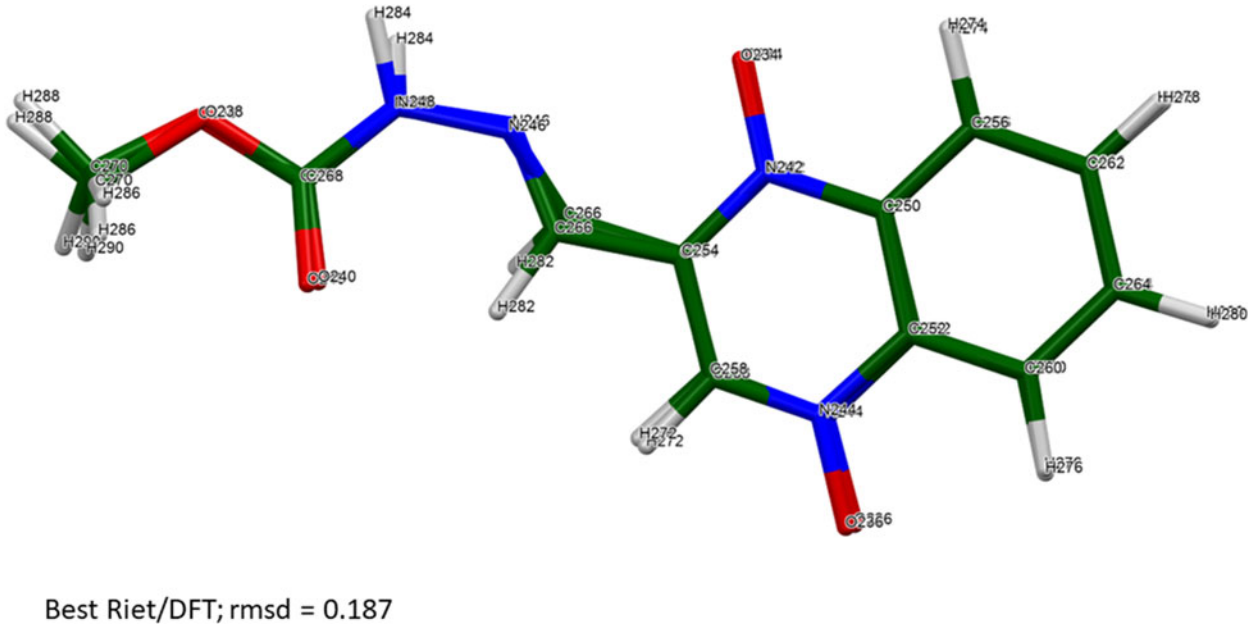

Figure 4. The best agreement (molecule 6) between the Rietveld-refined and DFT-optimized structures of a carbadox molecule. Image generated using Mercury (Macrae et al., 2020).

yielded by NBS*LATTICE (Himes and Mighel, 1985). Although the space group suggested by FOX was #14, two weak peaks adjacent to the lowest-angle strong peak are 100 and 10-1 (Figure 2) and thus violate the glide plane. The true space group is thus $P2_1$ (as suggested by EXPO2014), and thus, there are eight molecules in the asymmetric unit. A reduced cell search in the Cambridge Structural Database (Groom et al., 2016) yielded two hits but no carbadox derivatives.

The initial $P2_1/n$ cell was transformed to the *c*-unique supercell with *Materials Studio* (Dassault Systèmes, 2022) using the matrices suggested by NBS*LATTICE. The space group was set to *P1*, and the unit cell was converted to the conventional *b*-unique cell using the matrix [100/00-1/010]. A

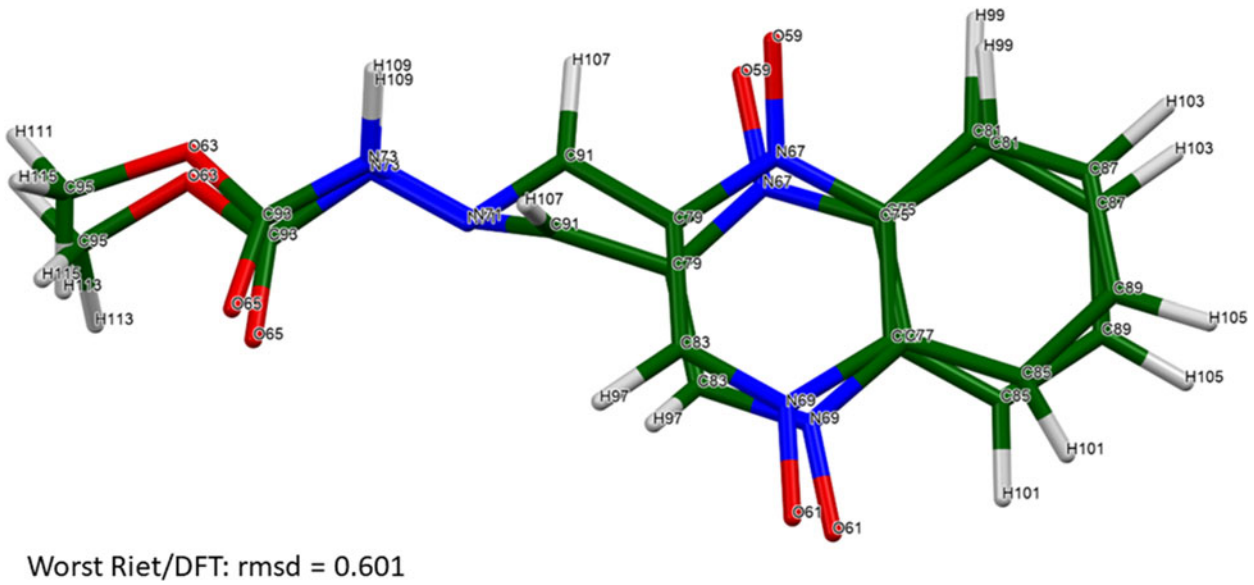

Figure 5. The worst agreement (molecule 3) between the Rietveld-refined and DFT-optimized structures of a carbadox molecule. Image generated using Mercury (Macrae et al., 2020).

https://doi.org/10.1017/S0885715624000083 Published online by Cambridge University Press

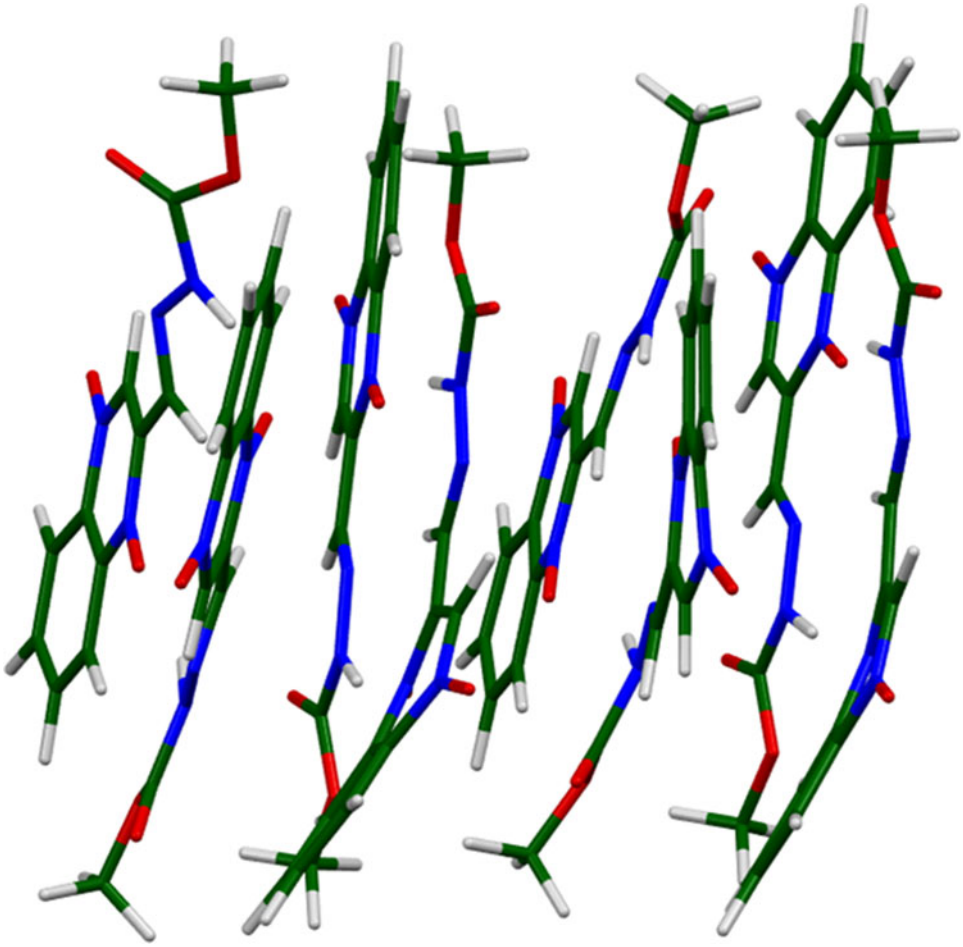

Figure 6. The asymmetric unit of carbadox. Image generated using Mercury (Macrae et al., 2020).

coordinate transformation of $x + 1/4,y,z + 1/4$ was applied, and the space group was changed to $P2_1$.

Rietveld refinement was carried out using GSAS-II (Toby and Von Dreele, 2013). Only the 2.0–25.0° portion of the pattern was included in the refinement ($d_{min} = 1.058$ Å). Initial refinements used eight rigid carbadox molecules but yielded some close intermolecular contacts. Thus, all non-H bond distances and angles were subjected to restraints (plus planar restraints for the dioxidoquinoxaline ring systems) based on a Mercury/Mogul Geometry check (Bruno *et al.*, 2004; Sykes et al., 2011). The Mogul average and standard deviation for each quantity were used as the restraint parameters. The restraints contributed 8.6% to the final χ^2. The hydrogen atoms were included in calculated positions, which were recalculated during the refinement using Materials Studio (Dassault Systèmes, 2022). The U_{iso} of the heavy atoms were grouped by chemical similarity. The U_{iso} for the H atoms were fixed at 1.3× the U_{iso} of the heavy atoms to which they are attached. A 6th-order spherical harmonic preferred orientation model was used; the texture index was 1.149. The peak profiles were described using a uniaxial size broadening model, with 001 as the unique axis. The background was modeled using a 3-term shifted Chebyshev polynomial and a peak at 6.27° 2θ to model the scattering from the Kapton capillary and any amorphous component.

The final refinement of 476 variables using 23,037 observations and 384 restraints yielded the residuals $R_{wp} = 0.2156$ and (Goodness of Fit (GOF) = 3.87). The residuals are higher than would normally be considered acceptable, but this is a very large refinement using relatively limited data. The largest

TABLE III. Root-mean-square Cartesian displacements (Å) between the independent carbadox molecules in the DFT-optimized structure.

Molecule	11–57 odd	22–58 even	359–115 odd	460–116 even	5233–289 odd	6234–290 even	7291–347 odd	8292–348 even
1	–	0.508	0.642	0.732	0.372	0.549	0.612	0.591
2		–	0.549	0.567	0.229	0.657	0.493	0.544
3			–	0.124	0.634	0.881	0.691	0.746
4				–	0.680	0.954	0.733	0.798
5					–	0.559	0.507	0.508
6						–	0.362	0.281
7							–	0.120
8								–

https://doi.org/10.1017/S0885715624000083 Published online by Cambridge University Press

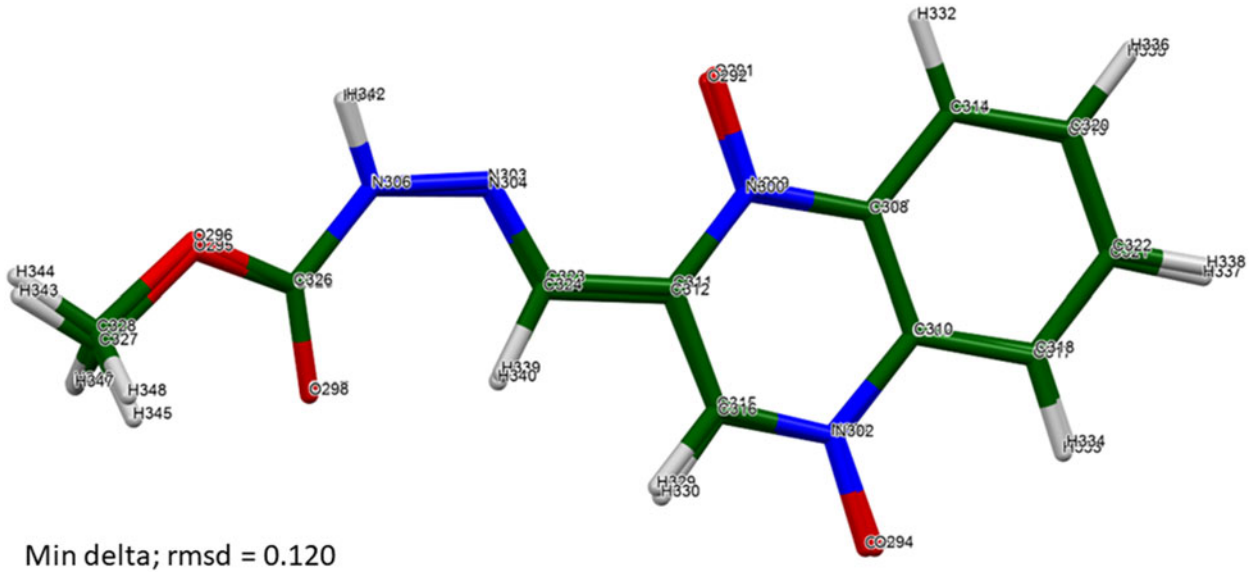

Figure 7. The two carbadox molecules (7 and 8) are most similar. Image generated using Mercury (Macrae et al., 2020).

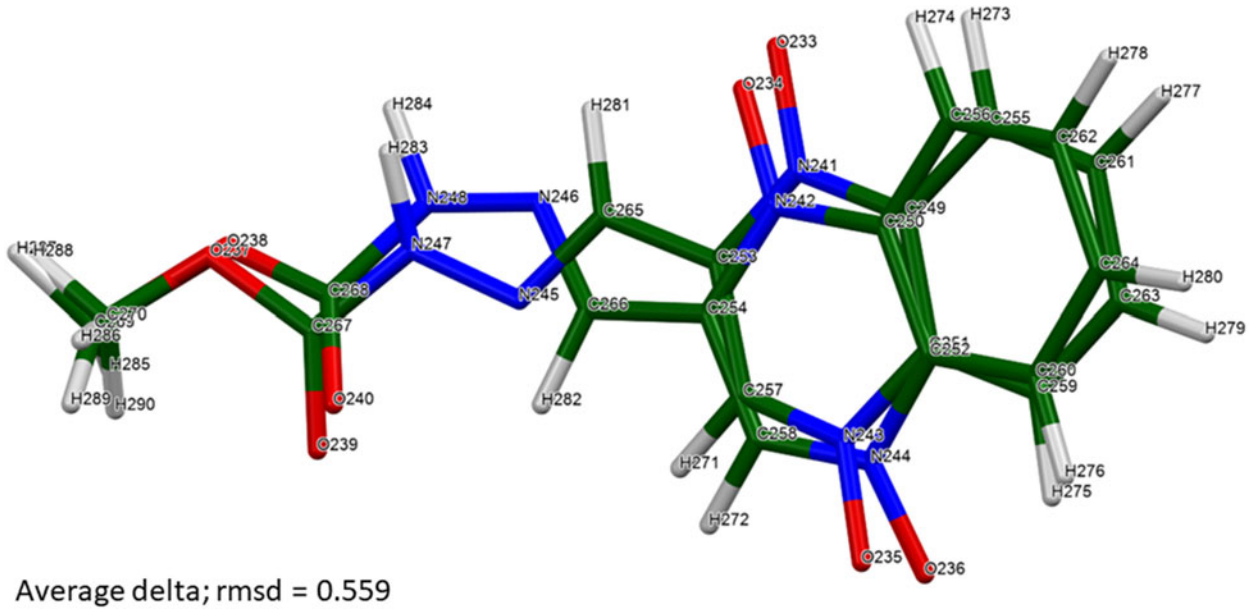

Figure 8. The two molecules (5 and 6) represent the average similarity between carbadox molecules. Image generated using Mercury (Macrae et al., 2020).

peak (1.35 Å from C319) and hole (2.13 Å from O292) in the difference Fourier map were 1.82(41) and –1.80(41) eÅ^{-3}, respectively. The largest errors in the difference plot (Figure 3) are in the intensities of some of the peaks and probably represent an incomplete model for the preferred orientation. There are also some unindexed peaks, indicating the presence of at least one crystalline impurity.

The structure was optimized (fixed experimental unit cell) with density functional techniques using VASP (Kresse and Furthmüller, 1996) through the MedeA graphical interface (Materials Design, 2016). The calculations were carried out on 16 2.4 GHz processors (each with 4 Gb RAM) of a 64-processor HP Proliant DL580 Generation 7 Linux cluster at North Central College. The calculation used the GGA-PBE functional, a plane wave cutoff energy of 400.0 eV, and a k-point spacing of 0.5 Å^{-1} leading to a 1 × 1 × 1 mesh, and took ∼295 h. The system is a semiconductor, with a direct band gap of 1.440 eV. A single-point density functional calculation (fixed experimental cell) and population analysis were carried out using CRYSTAL23 (Erba et al., 2023). The basis sets for the H, C, N, and O atoms in the calculation were those of Gatti et al. (1994). The calculation was run on a 3.5 GHz PC using eight k-points and the B3LYP functional, and took ∼30 h. Neither PLATON (Spek, 2009, 2020) nor Materials Studio detected additional symmetry in the refined or optimized structure, so the space group seems to be $P2_1$.

To modify the degree of preferred orientation, several different specimens of carbadox were prepared and measured on a Bragg-Brentano diffractometer with Cu radiation using flat plate specimens and on a Debye–Scherrer diffractometers with Mo radiation using capillary specimens.

https://doi.org/10.1017/S0885715624000083 Published online by Cambridge University Press

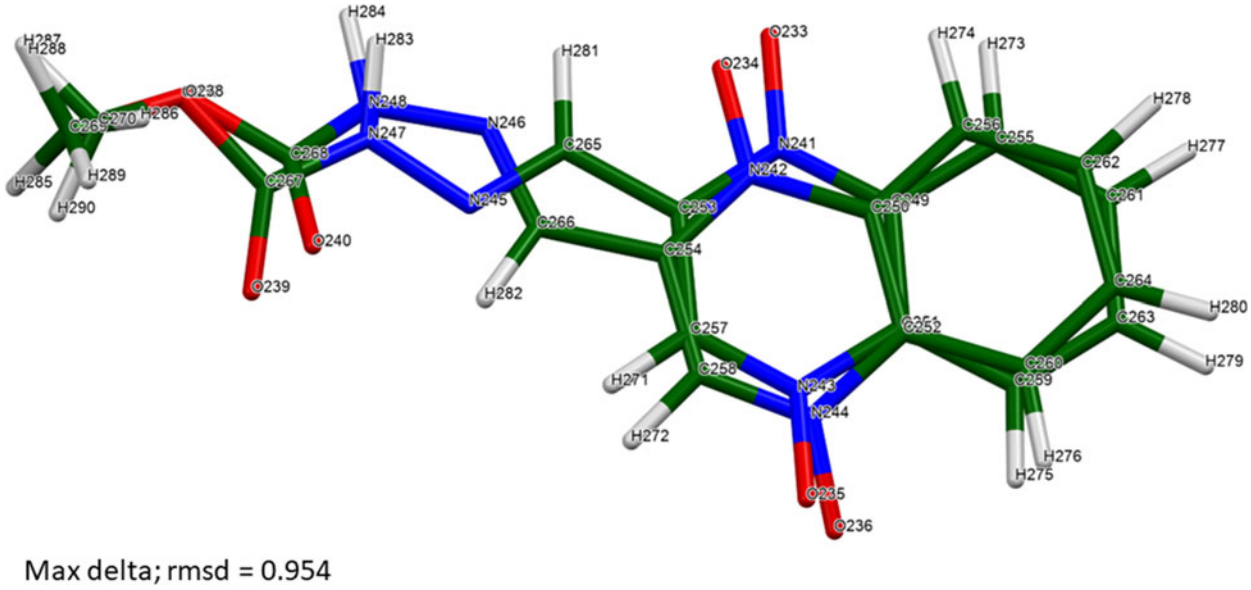

Figure 9. The two carbadox molecules (4 and 5) are most different. Image generated using Mercury (Macrae et al., 2020).

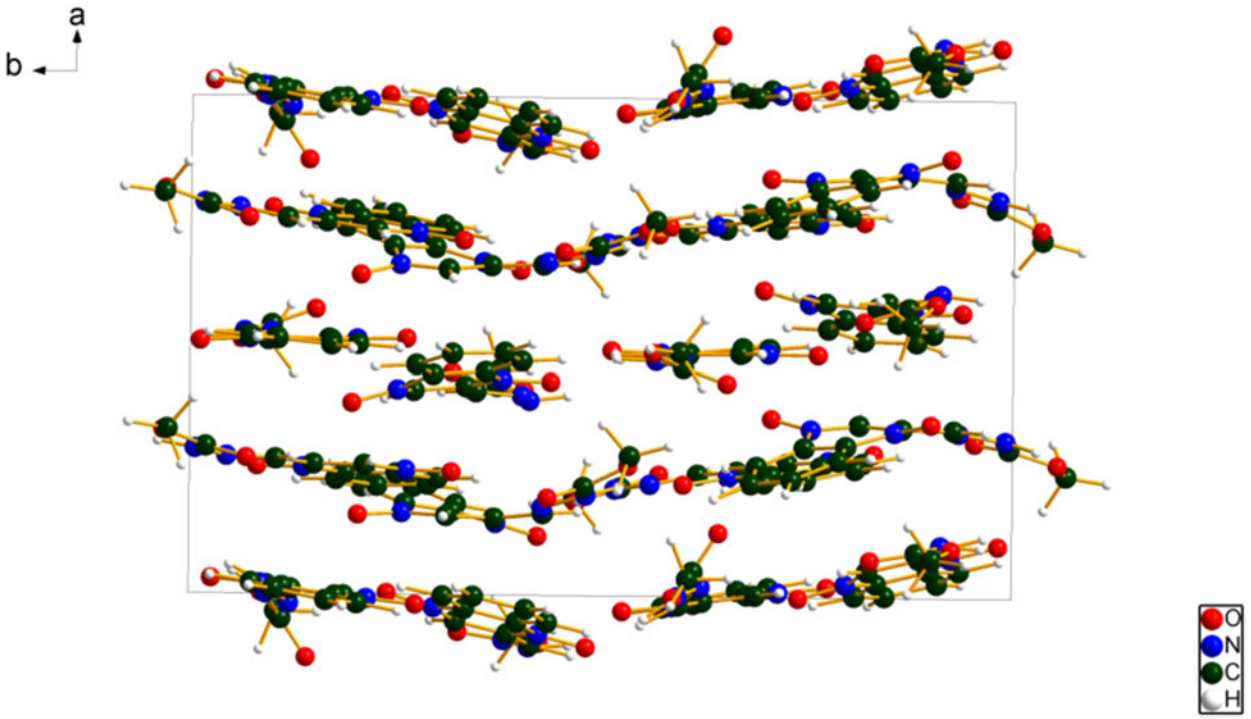

Figure 10. The crystal structure of carbadox, viewed down the *c*-axis. Image generated using Diamond (Crystal Impact, 2022).

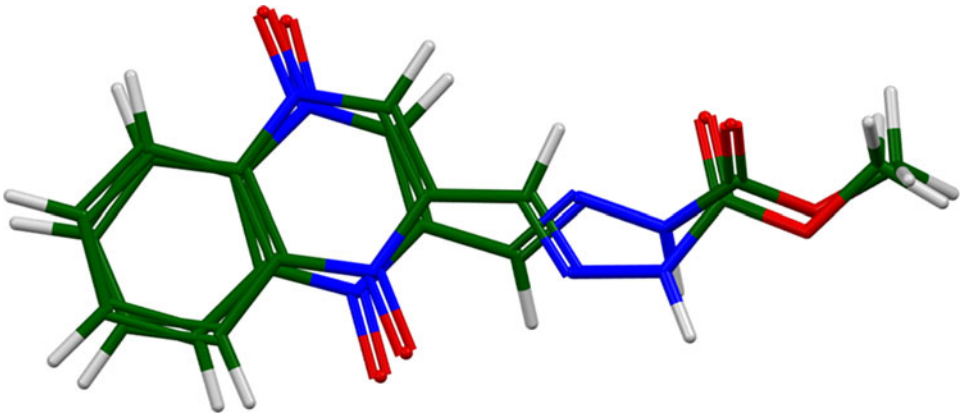

Figure 11. Molecules 1 and 8 illustrate the two different configurations of the carbadox molecule.

https://doi.org/10.1017/S0885715624000083 Published online by Cambridge University Press

TABLE IV. Hydrogen bonds (CRYSTAL23) in carbadox.

H-bond	D–H, Å	H···A, Å	D···A, Å	D–H···A,◦	Overlap, *e*	*E*, kcal/mol
Amino donors						
N15–H51···O233	1.037	1.831	2.767	159.8	0.049	5.1
N16–H52···O234	1.037	1.831	2.810	155.9	0.049	5.1
N73–H109···O292	1.031	2.338	3.340	163.7	0.022	3.4
N74–H110···O291	1.038	1.904	2.923	166.4	0.046	4.9
N247–H283···O1	1.038	1.764	2.686	145.6	0.055	5.4
N248–H284···O2	1.037	1.681	2.578	141.9	0.067	6.0
N305–H341···O60	1.033	1.687	2.685	161.1	0.054	5.4
N306–H342···O59	1.042	1.627	2.631	160.1	0.070	6.1
Aromatic C–H donors						
C23–H41···O237	1.088	2.310	3.360	161.8	0.019	
C24–H42···O2	1.089	2.350[a]	2.712	97.3	0.016	
C81–H99···O59	1.088	2.405[a]	2.739	95.9	0.012	
C81–H99···O296	1.088	2.450	3.514	165.5	0.018	
C82–H100···O60	1.097	2.455[a]	2.759	95.6	0.010	
C255–H273···O5	1.087	2.413	3.335	141.7	0.014	
C255–H273···O233	1.087	2.429[a]	2.761	95.9	0.010	
C256–H274···O6	1.087	2.377	3.435	164.1	0.020	
C256–H274···O234	1.087	2.422[a]	2.755	95.9	0.013	
C313–H331···O64	1.086	2.305	3.312	153.3	0.018	
C313–H331···O291	1.086	2.417[a]	2.751	96.0	0.012	
C314–H332···O292	1.084	2.413[a]	2.741	95.7	0.013	
C27–H43···O239	1.089	2.078	3.046	146.6	0.033	
C27–H43···O3	1.089	2.426[a]	2.757	95.7	0.019	
C28–44···O240	1.086	2.163	2.981	130.2	0.023	
C28–H44···O4	1.086	2.467[a]	2.778	94.8	0.013	
C85–H101···O61	1.089	2.467[a]	2.782	95.0	0.018	
C84–H98···N72	1.085	2.500[a]	2.768	92.1	0.009	
C257–H271···N245	1.086	2.533[a]	2.817	93.6	0.014	
C258–H272		–				
C317–H353···O65	1.087	2.419	3.099	119.2	0.013	
C317–H353···O293	1.087	2.431[a]	2.766	96.1	0.020	
C318–H334···O294	1.087	2.425[a]	2.756	95.8	0.021	
C318–H334···O66	1.087	2.496	3.174	119.4	0.011	
Vinyl donors						
C33–H49···O233	1.094	2.257	3.132	135.4	0.016	
C34–H50···O2	1.095	2.388[a]	2.727	95.9	0.012	
C91–H107···O59	1.098	2.376[a]	2.719	96.0	0.012	
C91–H107···N304	1.098	2.998	4.053	161.3	0.010	
C92–H108···O60	1.097	2.455[a]	2.772	94.8	0.010	
C92–H108···N303	1.097	2.840	3.904	163.4	0.011	
C265–H281		–				
C266–H282···O240	1.095	2.190[a]	2.859	117.0	0.016	
C323–H339···O297	1.094	2.122[a]	2.860	122.3	0.011	
C323–H339···C325	1.094	2.569[a]	2.882	95.1	0.011	
C324–H340···O298	1.095	2.165[a]	2.877	120.3	0.017	
Methyl donors						
C38–H54···O62	1.094	2.229	3.227	141.4	0.010	
C38–H54···O8	1.094	2.460[a]	2.674	89.9	0.011	
C38–H56···O236	1.098	2.521	3.289	126.0	0.014	
C96–H112···O61	1.094	2.299	3.333	157.0	0.015	
C269–H285···O294	1.099	2.166	3.257	171.5	0.036	

[a]Intramolecular.

III. RESULTS AND DISCUSSION

Although not a protein, the crystal structure of carbadox is a very large one to be solved and refined using powder diffraction data. Searches of the Cambridge Structural Database for high-Z' powder structures yielded the results as shown in Table I. Only 9.7% of the 3391 powder structures have $Z' > 1$, and only two have $Z' = 8$. These two molecules are 5,7-dihydroxy-2-phenyl-4H-chromen-4-one (Chrysin, Chadha et al., 2017; IYIWIY) and perdeutero-4-methylpyridine-*N*-oxide (Damay et al., 2006; ZZZVCO03). Both of these are also nearly planar molecules.

The root-mean-square Cartesian displacements between the Rietveld-refined and DFT-optimized molecules lie partly within and partly outside the normal range for correct structures (Table II; van de Streek and Neumann, 2014). The best agreement (root mean square displacement (rmsd) = 0.187 Å) is for molecule 6 (Figure 4), and the worst is for molecule 3 (rmsd = 0.601 Å; Figure 5). The refinement of a very large number of parameters using relatively limited data on

https://doi.org/10.1017/S0885715624000083 Published online by Cambridge University Press

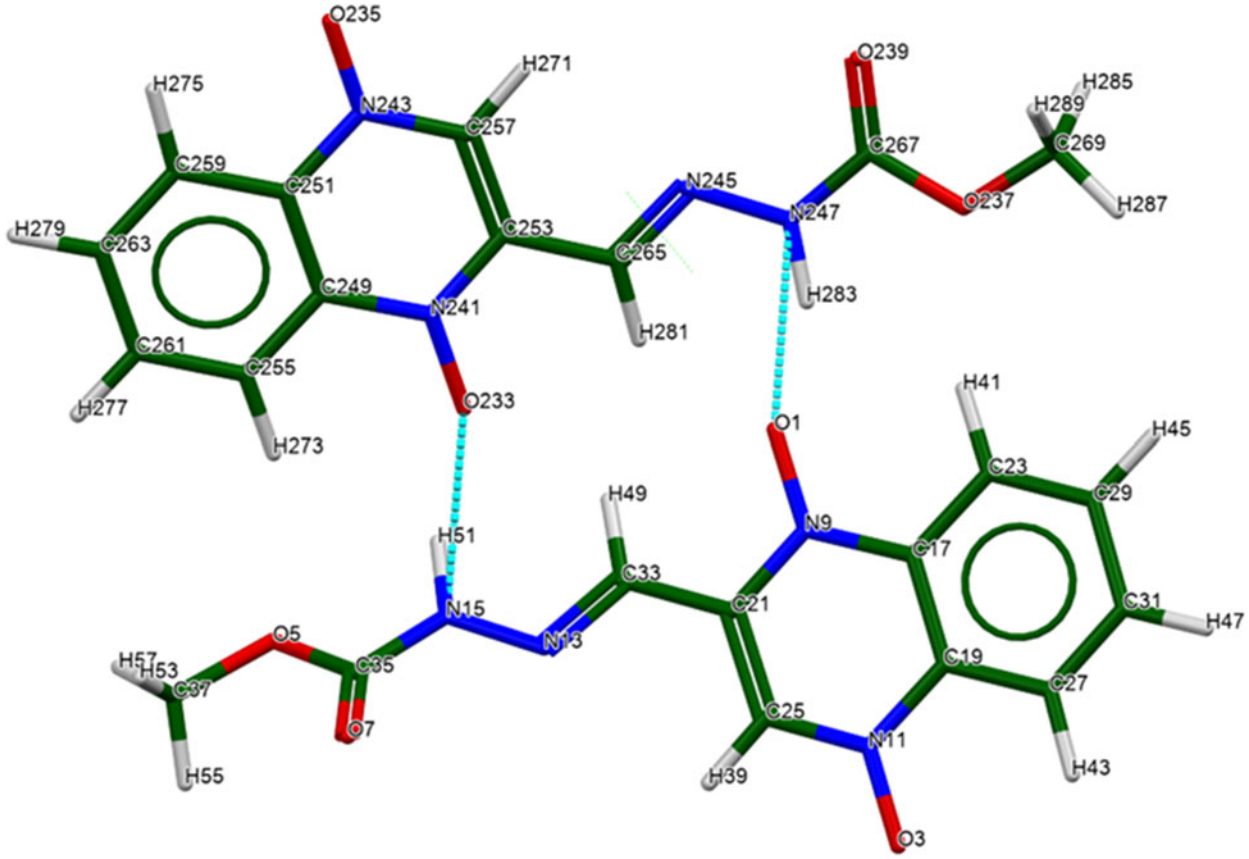

Figure 12. The hydrogen bonds between molecules 1 and 5. Image generated using Mercury (Macrae et al., 2020).

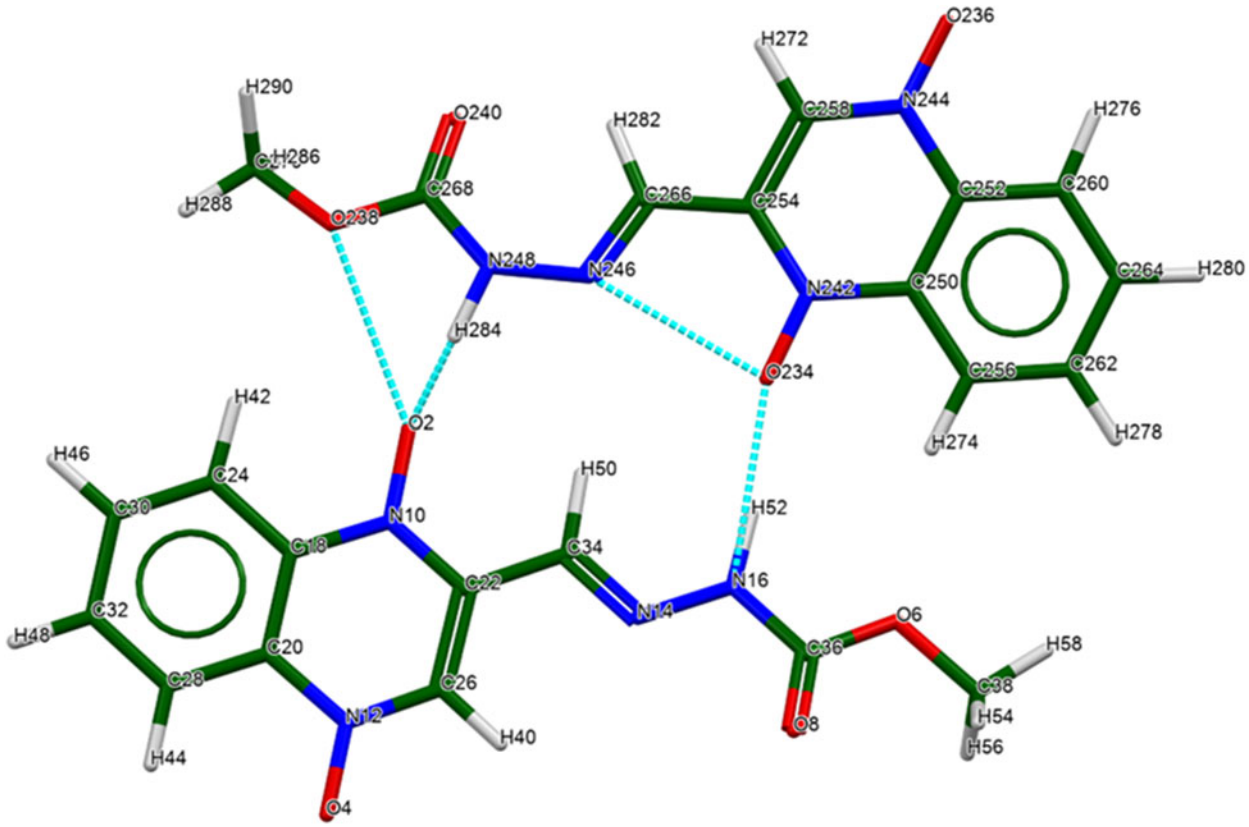

Figure 13. The hydrogen bonds between molecules 2 and 6. Image generated using Mercury (Macrae et al., 2020).

https://doi.org/10.1017/S0885715624000083 Published online by Cambridge University Press

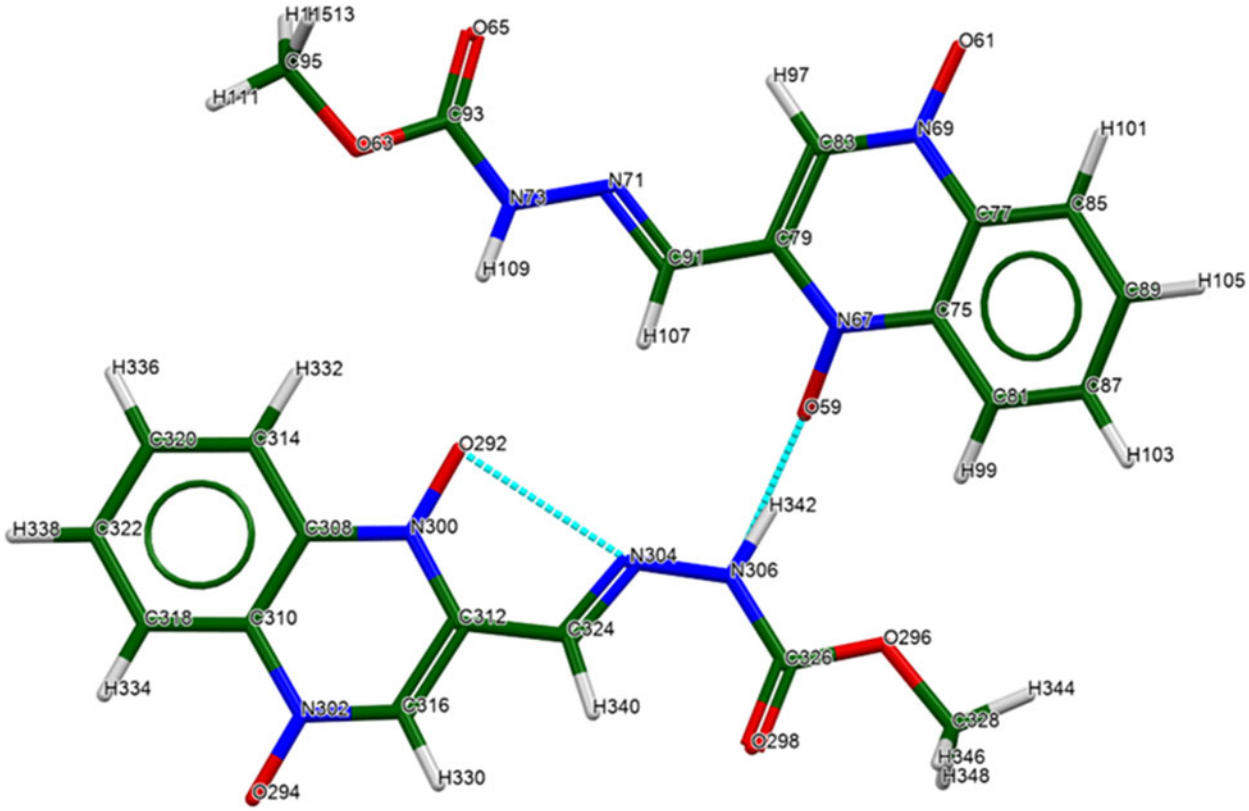

Figure 14. The hydrogen bonds between molecules 3 and 8. Image generated using Mercury (Macrae et al., 2020).

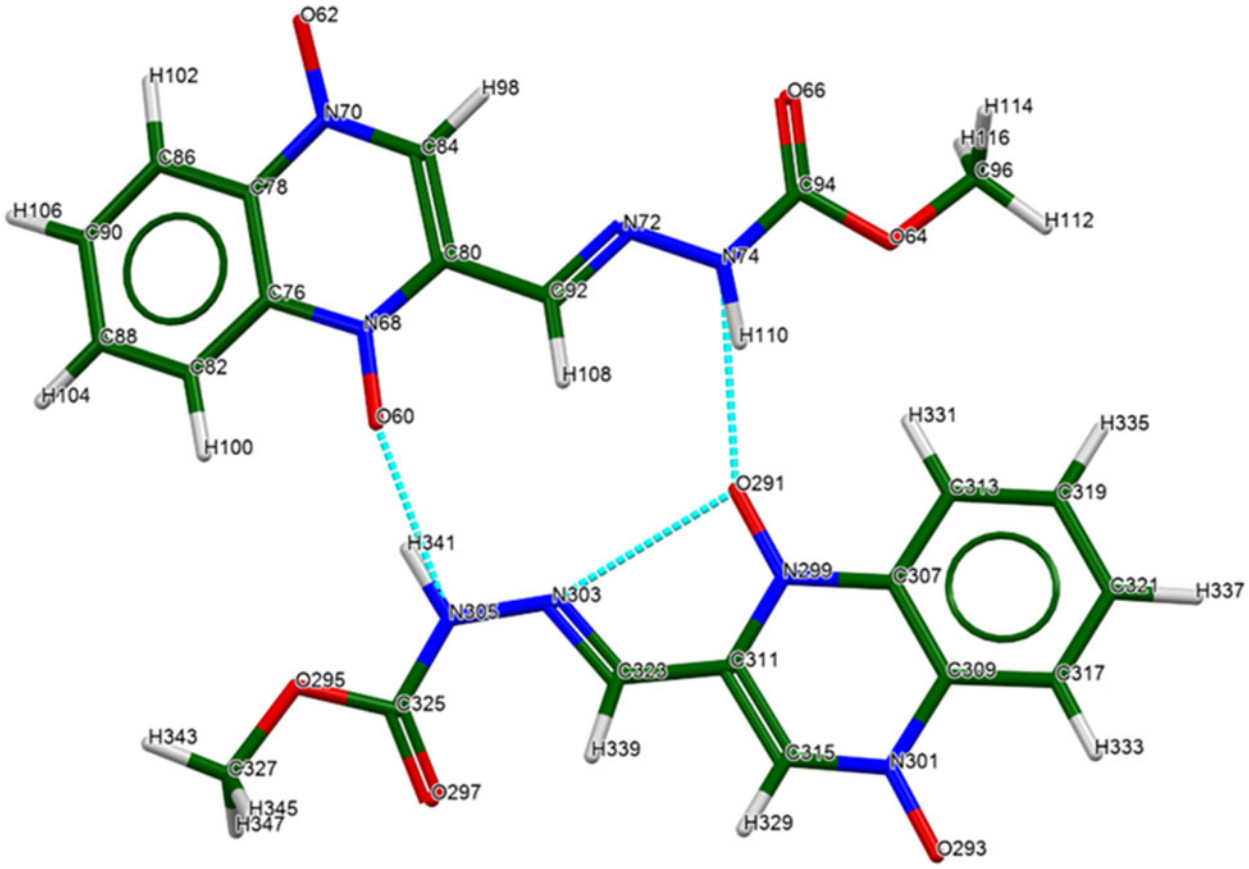

Figure 15. The hydrogen bonds between molecules 4 and 7. Image generated using Mercury (Macrae et al., 2020).

https://doi.org/10.1017/S0885715624000083 Published online by Cambridge University Press

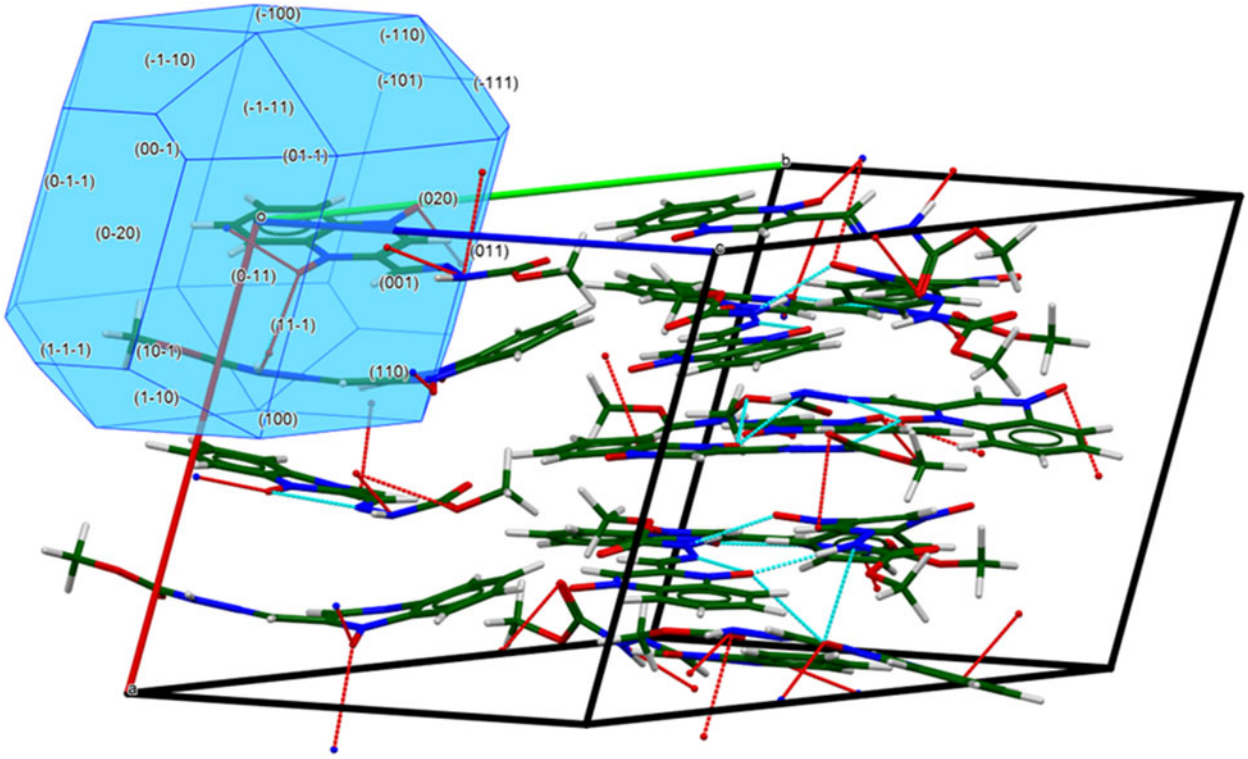

Figure 16. The BFDH crystal morphology of carbadox. The red, green, and blue unit cell edges are the *a*-, *b*-, and *c*-axes, respectively. Image generated using Mercury (Macrae et al., 2020).

an oriented specimen almost certainly means that the refined structure is less accurate and less precise than usual, so such disagreements are to be expected. As expected, the side chains of the carbadox molecules deviate the most from the overall molecular plane. There is the possibility of tautomerism in the carbadox molecule, and there might be more than one tautomer coexisting in the crystalline form. The remaining discussion will focus on the DFT-optimized structure, as it is likely more accurate. The asymmetric unit is illustrated in Figure 6.

The eight independent molecules vary in conformation (Table III). The best, average, and worst agreements are illustrated in Figures 7–9.

The crystal structure is characterized by roughly parallel stacking of the carbadox molecules parallel to the *bc*-plane (Figure 10). The hydrogen bonds (discussed below) link the

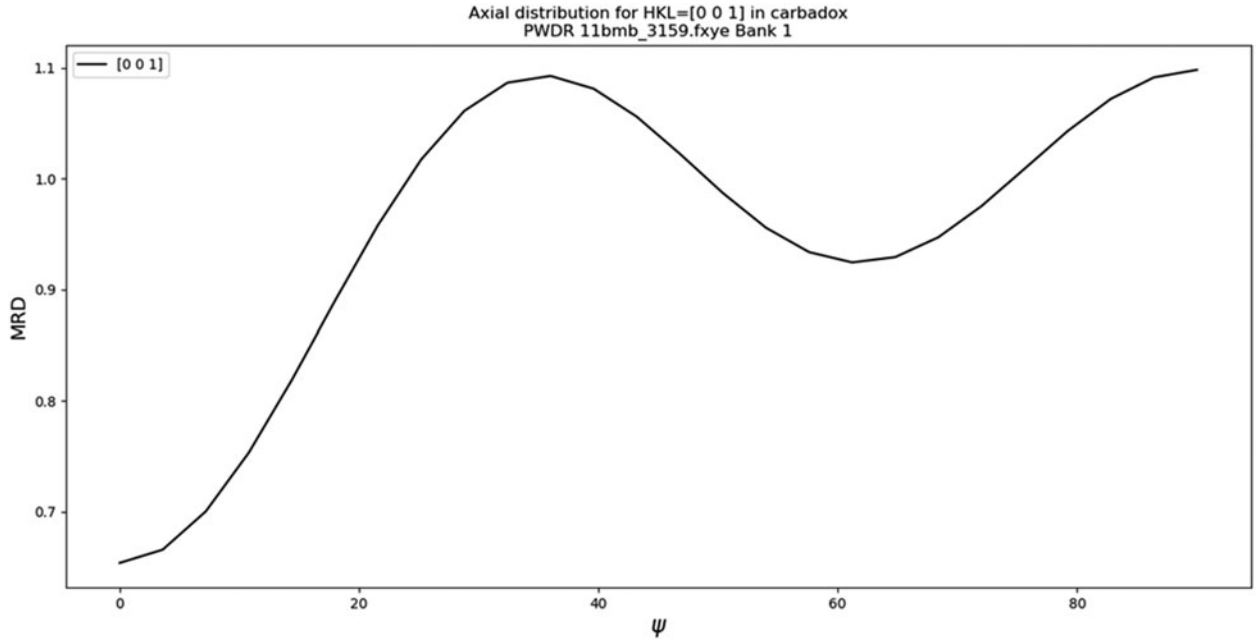

Figure 17. The axial distribution of the 001 vector in the capillary specimen of carbadox.

https://doi.org/10.1017/S0885715624000083 Published online by Cambridge University Press

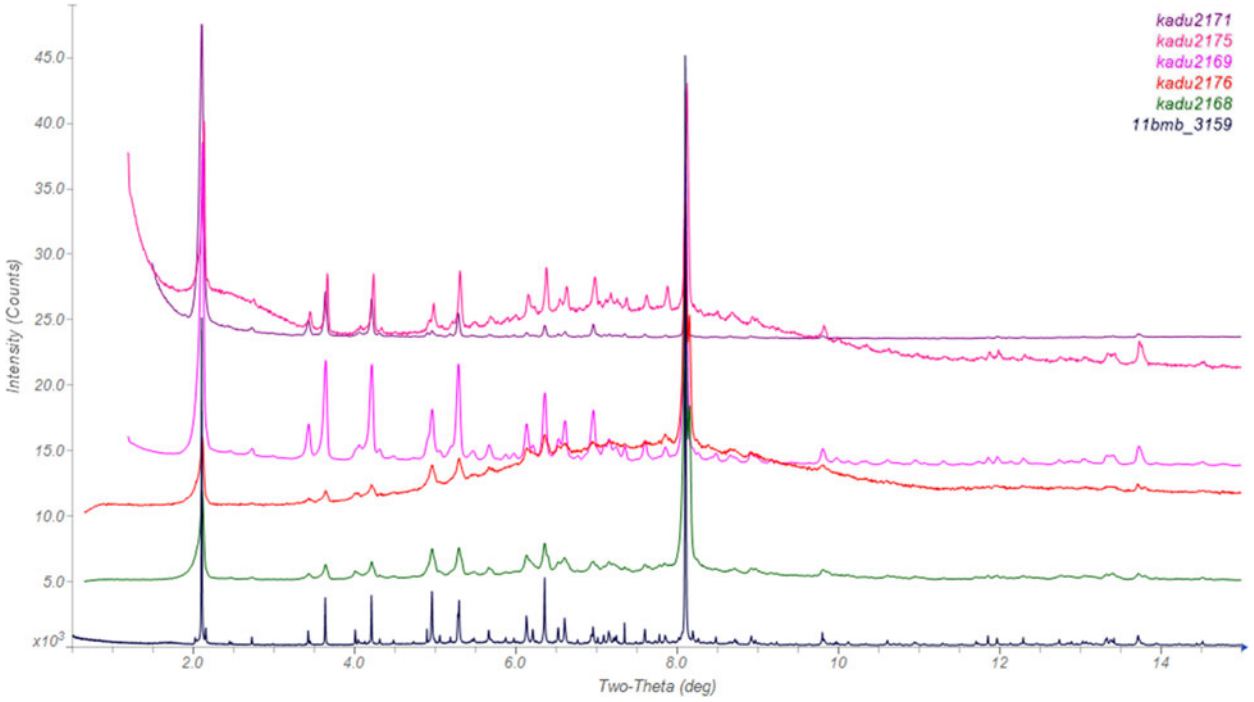

Figure 18. Variation in texture with different specimen preparations (see Table V for specimen mounting methods). The colors of the file names in the upper right match those of the diffraction patterns. The laboratory patterns have been converted to the synchrotron wavelength using JADE Pro. Image generated using JADE Pro (MDI, 2023).

molecules both within and between the planes. The *Mercury* Aromatics Analyser indicates two moderate interactions with distances of 3.79 and 5.81 Å between molecules 2/4 and 1/4, respectively, and eight weaker interactions with longer distances.

Almost all of the bond distances, bond angles, and torsion angles fall within the normal ranges indicated by a Mercury Mogul Geometry check (Macrae et al., 2020). Two of the N=N double bonds (N16–N14 = 1.331 Å, average = 1.377 (12) Å, *Z*-score = 3.7 and N74–N72 = 1.339 Å, *Z*-score = 3.0) are flagged as unusual. The angles between the side chain and the ring system (C33–C21–N9 and equivalents) range from 117.1 to 125.8° and are all flagged as unusual. The average angle for this type is 120.3(3)°, but the population is small. The standard deviation on the average is exceptionally small, resulting in inflated *Z*-scores ranging from 6.1 to 14.0. Some of the torsion angles between the ring system and the side chain (N13–C33–C21–N9 and equivalents) are flagged as unusual but with few hits. Some of the N–N torsion angles (C268–N248–N246–C266 and equivalents) are also flagged as unusual. The carbadox molecule is indeed fairly unusual.

Quantum chemical geometry optimization of the isolated individual molecules (DFT/B3LYP/6-31G*/water) using Spartan '20 (Wavefunction, 2022) indicated that there are two configurations of carbadox molecules (Figure 11) that are related by an approximate 180° rotation about the C–C bond between the ring system and the side chain: molecules 1–5 and molecules 6–8. Molecules 6–8 are approximately 6.3 kcal/mol higher in energy than the other configuration. The local minimum-energy molecules are all planar, while the ones in the crystal structure deviate significantly from planarity.

Hydrogen bonds are prominent in the crystal structure (Table IV). Each of the amino groups (the only classical donor in the molecule) forms a N–H···O hydrogen bond to an oxygen atom of the 1,4-dioxidoquinoxaline ring system of another molecule. The result is four pairs of hydrogen-bonded molecules, which form rings with graph set *R2,2 (14)* (Etter, 1990; Bernstein et al., 1995; Shields et al., 2000) (Figures 12–15). These hydrogen-bonded pairs (molecules 1/5, 2/6, 3/8, 4/7) lie in the planes of the ring stacking. There are a variety of intra- and intermolecular C–H···O and C–H···N hydrogen bonds. The intermolecular ones link the molecules perpendicular to the stacking planes.

The Bravais–Friedel–Donnay–Harker (BFDH; Bravais, 1866; Friedel, 1907; Donnay and Harker, 1937) morphology suggests a slightly platy morphology for carbadox, with {001} as major faces, suggesting the possibility of preferred orientation. A 6th-order spherical harmonic preferred orientation model was included in the refinement. The refined texture index was 1.145, indicating that the preferred orientation was significant in this rotated capillary specimen. The distribution of the 001 axis is consistent with this picture (Figure 16), but the texture is more complex than a simple platy model

TABLE V. Texture indices in carbadox specimens.

Filename	Specimen mounting	Radiation	Texture index
11bmb_3159	1.5 mm Kapton capillary	Synchrotron	1.145
kadu2168	<325 mesh, 0.7 mm glass capillary	Mo	1.752
kadu2176	24.6% diluted with amorphous silica, 0.7 mm glass capillary	Mo	2.540
kadu2169	Si zero background cell	Cu	2.567
kadu2175	24.5% diluted with amorphous silica, Si zero background cell	Cu	7.94
kadu2171	Slurry mount, Si zero background cell	Cu	19.4

https://doi.org/10.1017/S0885715624000083 Published online by Cambridge University Press

(Figure 17). Other mountings of carbadox specimens yielded even greater preferred orientation (Figure 18 and Table V).

IV. DEPOSITED DATA

The powder pattern of carbadox from this synchrotron data set has been submitted to ICDD for inclusion in the Powder Diffraction File. The Crystallographic Information Framework (CIF) files containing the results of the Rietveld refinement (including the raw data) and the DFT geometry optimization were deposited with the ICDD. The data can be requested at pdj@icdd.com.

ACKNOWLEDGEMENTS

The use of the Advanced Photon Source at Argonne National Laboratory was supported by the U. S. Department of Energy, Office of Science, Office of Basic Energy Sciences under Contract No. DE-AC02-06CH11357. This work was partially supported by the International Centre for Diffraction Data. We thank Lynn Ribaud and Saul Lapidus for their assistance in the data collection.

CONFLICTS OF INTEREST

The authors have no conflicts of interest to declare.

REFERENCES

Antao, S. M., I. Hassan, J. Wang, P. L. Lee, and B. H. Toby. 2008. "State-of-the-Art High-Resolution Powder X-Ray Diffraction (HRPXRD) Illustrated with Rietveld Refinement of Quartz, Sodalite, Tremolite, and Meionite." *Canadian Mineralogist* 46: 1501–9.

Bernstein, J., R. E. Davis, L. Shimoni, and N. L. Chang. 1995. "Patterns in Hydrogen Bonding: Functionality and Graph Set Analysis in Crystals." *Angewandte Chemie International Edition in English* 34: 1555–73.

Bravais, A. 1866. *Etudes Cristallographiques*. Paris, Gauthier Villars.

Bruno, I. J., J. C. Cole, M. Kessler, J. Luo, W. D. S. Motherwell, L. H. Purkis, B. R. Smith, R. Taylor, R. I. Cooper, S. E. Harris, and A. G. Orpen. 2004. "Retrieval of Crystallographically-Derived Molecular Geometry Information." *Journal of Chemical Information and Computer Sciences* 44: 2133–44.

Chadha, R., Y. Bhalla, A. Nandan, K. Chadha, and M. Karan. 2017. "Chrysin Cocrystals: Characterization and Evaluation." *Journal of Pharmaceutical and Biomedical Analysis* 134: 361–71.

Crystal Impact. 2022. *Diamond. V. 4.6.8. Crystal Impact – Dr. H. Putz & Dr. K. Brandenburg*. Bonn: Windows.

Damay, F., A. Carretero-Genevrier, A. Cousson, J. Rodriguez-Carvajal, W. Van Beek, and F. Fillaux. 2006. "Synchrotron and Neutron Diffraction Study of 4-Methylpyridine-N-Oxide at Low Temperature." *Acta Crystallographica Section B: Structural Science* 62: 627–33.

Dassault Systèmes. 2022. *BIOVIA Materials Studio 2023*. San Diego, CA, BIOVIA.

Donnay, J. D. H., and D. Harker. 1937. "A New Law of Crystal Morphology Extending the Law of Bravais." *American Mineralogist* 22: 446–67.

Erba, A., J. K. Desmaris, S. Casassa, B. Civalleri, L. Donà, I. J. Bush, B. Searle, L. Maschio, L.-E. Daga, A. Cossard, C. Ribaldone, E. Ascrizzi, N. L. Marana, J.-P. Flament, and B. Kirtman. 2023. "CRYSTAL23: A Program for Computational Solid State Physics and Chemistry." *Journal of Chemical Theory and Computation* 19: 6891–932. doi:10.1021/acs.jctc.2c00958.

Etter, M. C. 1990. "Encoding and Decoding Hydrogen-Bond Patterns of Organic Compounds." *Accounts of Chemical Research* 23: 120–6.

Favre-Nicolin, V., and R. Černý. 2002. "FOX, Free Objects for Crystallography: A Modular Approach to ab initio Structure Determination from Powder Diffraction." *Journal of Applied Crystallography* 35: 734–43.

Friedel, G. 1907. "Etudes sur la loi de Bravais." *Bulletin de la Société Française de Minéralogie* 30: 326–455.

Gates-Rector, S., and T. N. Blanton. 2019. "The Powder Diffraction File: A Quality Materials Characterization Database." *Powder Diffraction* 39: 352–60.

Gatti, C., Saunders, V. R., and C., Roetti (1994). "Crystal-Field Effects on the Topological Properties of the Electron-Density in Molecular Crystals - the Case of Urea." *Journal of Chemical Physics* 101: 10686–96.

Groom, C. R., I. J. Bruno, M. P. Lightfoot, and S. C. Ward. 2016. "The Cambridge Structural Database." *Acta Crystallographica Section B: Structural Science, Crystal Engineering and Materials* 72: 171–9.

Himes, V. L., and A. D. Mighel. 1985. *NBS*LATTICE: a Program to Analyze Lattice Relationships*. Gaithersburg, MD, National Bureau of Standards.

Kaduk, J. A., C. E. Crowder, K. Zhong, T. G. Fawcett, and M. R. Suchomel. 2014. "Crystal Structure of Atomoxetine Hydrochloride (Strattera), $C_{17}H_{22}NOCl$." *Powder Diffraction* 29: 269–73.

Kim, S., J. Chen, T. Cheng, A. Gindulyte, J. He, S. He, Q. Li, B. A. Shoemaker, P. A. Thiessen, B. Yu, L. Zaslavsky, J. Zhang, and E. E. Bolton. 2023. "Pubchem 2023 Update." *Nucleic Acids Research* 51 (D1): D1373–80. doi:10.1093/nar/gkac956.

Kresse, G., and J. Furthmüller. 1996. "Efficiency of Ab-Initio Total Energy Calculations for Metals and Semiconductors Using a Plane-Wave Basis Set." *Computational Materials Science* 6: 15–50.

Lee, P. L., D. Shu, M. Ramanathan, C. Preissner, J. Wang, M. A. Beno, R. B. Von Dreele, L. Ribaud, C. Kurtz, S. M. Antao, X. Jiao, and B. H. Toby. 2008. "A Twelve-Analyzer Detector System for High-Resolution Powder Diffraction." *Journal of Synchrotron Radiation* 15: 427–32.

Louër, D., and A. Boultif. 2007. "Powder Pattern Indexing and the Dichotomy Algorithm." *Zeitschrift fur Kristallographie Supplements* 26: 191–6.

Louër, D., and A. Boultif. 2014. "Some Further Considerations in Powder Diffraction Pattern Indexing with the Dichotomy Method." *Powder Diffraction* 29: S7–12.

Macrae, C. F., I. Sovago, S. J. Cottrell, P. T. A. Galek, P. McCabe, E. Pidcock, M. Platings, G. P. Shields, J. S. Stevens, M. Towler, and P. A. Wood. 2020. "*Mercury 4.0*: From Visualization to Design and Prediction." *Journal of Applied Crystallography* 53: 226–35.

Materials Design. 2016. *MedeA 2.20.4*. Angel Fire, NM, Materials Design Inc.

MDI. 2023. *JADE Pro Version 8.8*. Livermore, CA, Materials Data.

O'Boyle, N. M., M. Banck, C. A. James, C. Morley, T. Vandermeersch, and G. R. Hutchison. 2011. "Open Babel: An Open Chemical Toolbox." *Journal of Chemical Informatics* 3: 33. doi:10.1186/1758-2946-3-33.

Shields, G. P., P. R. Raithby, F. H. Allen, and W. D. S. Motherwell. 2000. "The Assignment and Validation of Metal Oxidation States in the Cambridge Structural Database." *Acta Crystallographica Section B: Structural Science* 56: 455–65.

Spek, A. L. 2009. "Structure Validation in Chemical Crystallography." *Acta Crystallographica D* 65: 148–55.

Spek, A. L. 2020. "CheckCIF Validation Alerts: What They Mean and How To Respond." *Acta Crystallographica E* 76: 1–11.

Sykes, R. A., P. McCabe, F. H. Allen, G. M. Battle, I. J. Bruno, and P. A. Wood. 2011. "New Software for Statistical Analysis of Cambridge Structural Database Data." *Journal of Applied Crystallography* 44: 882–6.

Toby, B. H., and R. B. Von Dreele. 2013. "GSAS II: The Genesis of a Modern Open Source All Purpose Crystallography Software Package." *Journal of Applied Crystallography* 46: 544–9.

van de Streek, J., and M. A. Neumann. 2014. "Validation of Molecular Crystal Structures from Powder Diffraction Data with Dispersion-Corrected Density Functional Theory (DFT-D)." *Acta Crystallographica Section B: Structural Science, Crystal Engineering and Materials* 70: 1020–32.

Wang, J., B. H. Toby, P. L. Lee, L. Ribaud, S. M. Antao, C. Kurtz, M. Ramanathan, R. B. Von Dreele, and M. A. Beno. 2008. "A Dedicated Powder Diffraction Beamline at the Advanced Photon Source: Commissioning and Early Operational Results." *Review of Scientific Instruments* 79: 085105.

Wavefunction, Inc. 2022. Spartan '20. Version 1.1.4. Irvine, CA, Wavefunction Inc.